J. Fluid Mech. (2000), *vol.* 422, *pp.* 193–205. Printed in the United Kingdom

The von Neumann paradox in weak shock reflection

By A. R. ZAKHARIAN[1]†, M. BRIO[2], J. K. HUNTER[3] AND G. M. WEBB[1]

[1]Department of Planetary Sciences, University of Arizona, Tucson, AZ 85721, USA
[2]Department of Mathematics, University of Arizona, Tucson, AZ 85721, USA
[3]Department of Mathematics and ITD, University of California Davis, USA

(Received 4 January 2000 and in revised form 6 June 2000)

We present a numerical solution of the Euler equations of gas dynamics for a weak-shock Mach reflection in a half-space. In our numerical solutions, the incident, reflected, and Mach shocks meet at a triple point, and there is a supersonic patch behind the triple point, as proposed by Guderley. A theoretical analysis supports the existence of an expansion fan at the triple point, in addition to the three shocks. This solution is in complete agreement with the numerical solution of the unsteady transonic small-disturbance equations obtained by Hunter & Brio (2000), which provides an asymptotic description of a weak-shock Mach reflection. The supersonic patch is extremely small, and this work is the first time it has been resolved in a numerical solution of the Euler equations. The numerical solution uses six levels of grid refinement around the triple point. A delicate combination of numerical techniques is required to minimize both the effects of numerical diffusion and the generation of numerical oscillations at grid interfaces and shocks.

1. Introduction

Experimental observations (Bleakney & Taub 1949) of the irregular reflection of a weak shock off a wedge show a reflection pattern that closely resembles a single Mach reflection with a triple point. A theoretical analysis (Bleakney & Taub 1949; Henderson 1987; von Neumann 1963), however, implies that a standard triple-point configuration, in which three plane shocks and a plane contact discontinuity separated by constant states meet at a point, is impossible for sufficiently weak shocks. This apparent inconsistency is one of the 'von Neumann paradoxes' of weak shock reflection, which have been in dispute for over fifty years.

One way to resolve this apparent paradox was proposed by Guderley (1962). He suggested that there is a supersonic patch behind the triple point in a weak-shock Mach reflection, and that an expansion fan is generated at the triple point. The terms supersonic, subsonic and sonic refer to a local self-similar frame of reference, and are defined explicitly in the Appendix. A supersonic patch was recently found in numerical solutions of the unsteady transonic small-disturbance equations, which give an asymptotic description of the Mach reflection of weak shocks off thin wedges, Hunter & Brio (2000). Higher-resolution solutions of the unsteady transonic small-

† Present address: ACMS, Department of Mathematics, University of Arizona, Tucson, AZ 85721-0089, USA.

disturbance equations, computed in self-similar coordinates, are shown in Tesdall & Hunter (2000).

The unsteady transonic small-disturbance equations are a significant simplification of the Euler equations. For example, vorticity and entropy variations are neglected in this approximation. In this paper, we present a numerical solution of the Euler equations for weak shock reflection in a half-space, using adaptive mesh refinement near the triple point. The solution contains a supersonic patch behind the triple point that is too small to be detected in previous numerical solutions of the Euler equations (Colella & Henderson 1990) or in previous experiments. The parameters in our full Euler solution are chosen to match the parameters in the unsteady transonic small-disturbance solution in Hunter & Brio (2000). The Euler solution and the unsteady transonic small-disturbance solution are remarkably similar, both qualitatively and quantitatively. This work therefore confirms the validity of the results obtained from the unsteady transonic small-disturbance equations, and shows that a supersonic patch does occur in solutions of the Euler equations.

The numerical solution we present here is for an oblique shock reflection in a half-space bounded by a solid wall, instead of for a shock reflection off a wedge. The simple half-space geometry enables us to keep the incident shock steady on the grid, which eliminates numerical diffusion and the generation of numerical noise at the shock. The overall features of the shock reflection pattern in the half-space and wedge geometries are very similar, but we did not obtain wedge solutions with the same resolution as the half-space solutions shown here. Nevertheless, the similarity between the large-scale structures of the solutions in the half-space and wedge geometries suggests that they have the same local structure near the triple point. This conclusion also follows from the matching argument in Hunter & Brio (2000), which shows that the local solution near the triple point has the same asymptotic description in both geometries.

2. Weak shock reflection

The fluid density ρ, velocity $\boldsymbol{u} = (u, v)$, and energy density e satisfy the compressible Euler equations,

$$\left.\begin{aligned} \rho_t + \nabla \cdot (\rho \boldsymbol{u}) &= 0, \\ (\rho \boldsymbol{u})_t + \nabla \cdot (\rho \boldsymbol{u} \otimes \boldsymbol{u} + p\boldsymbol{I}) &= 0, \\ \left(\rho\left(e + \tfrac{1}{2}\boldsymbol{u}^2\right)\right)_t + \nabla \cdot \left(\rho\left(e + \tfrac{1}{2}\boldsymbol{u}^2\right)\boldsymbol{u} + p\boldsymbol{u}\right) &= 0. \end{aligned}\right\} \tag{2.1}$$

We use an ideal gas equation of state,

$$e(p, \rho) = \frac{1}{\gamma - 1}\frac{p}{\rho},$$

where the ratio of specific heats γ is taken to be $5/3$.

For a gas with a given equation of state, there are two parameters in the shock reflection problem:

$$M = \text{Mach number of the incident shock},$$
$$\theta_w = \text{angle of shock to wall normal}.$$

When the shock strength $M - 1$ and the angle θ_w of the shock to the wall normal are related by

$$M - 1 = O(\theta_w^2) \quad \text{as} \quad \theta_w \to 0, \tag{2.2}$$

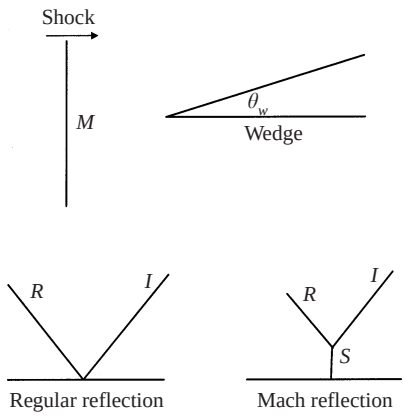

FIGURE 1. Schematic diagram of weak-shock reflection patterns.

a pattern that resembles a single Mach reflection is observed. This pattern is illustrated schematically in figure 1. Three shocks – the incident, reflected, and the Mach shocks – meet at a triple point.

We solve the two-dimensional, compressible Euler equations in a half-space $-\infty < x < \infty$, and $y > 0$. The initial data at $t = 0$ correspond to an oblique plane shock,

$$(\rho, \boldsymbol{u}, p) = \begin{cases} (\rho_R, \boldsymbol{u}_R, p_R), & x > (\tan\theta_w)y \\ (\rho_L, \boldsymbol{u}_L, p_L), & x < (\tan\theta_w)y, \end{cases}$$

where the left- and right-hand states are connected by the Rankine–Hugoniot jump conditions for a shock with Mach number M. The boundary condition on the wall $y = 0$ is

$$v = 0,$$

where v is the y-velocity component. We suppose that $v_R = 0$, in which case $v_L \neq 0$ for $\theta_w > 0$. For $t > 0$, a reflected wave lifts off the wall as the initial data behind the shock adjusts to the no-flow boundary condition on the wall.

By reflection of the solution in the wall $y = 0$, this problem is equivalent to a three-state, two-dimensional Riemann problem for the compressible Euler equations. The solution is self-similar, and depends only on the variables

$$\xi = \frac{x}{c_0 t}, \qquad \eta = \frac{y}{c_0 t},$$

where c_0 is a constant with the dimensions of velocity. In the Appendix, we show that the sound wave characteristics of the self-similar Euler equations are given by

$$\frac{\mathrm{d}\eta}{\mathrm{d}\xi} = \tan\left(\arcsin(\mp c/\sqrt{\tilde{u}^2 + \tilde{v}^2}) + \arctan(\tilde{v}/\tilde{u})\right), \tag{2.3}$$

where $\tilde{u} = u - x/t$, $\tilde{v} = v - y/t$, and $c = (\gamma p/\rho)^{1/2}$ is the sound speed. The self-similar equations for the sound wave components are elliptic when $\tilde{u}^2 + \tilde{v}^2 < c^2$, and hyperbolic when $\tilde{u}^2 + \tilde{v}^2 > c^2$. The equations change type at the sonic line,

$$\tilde{u}^2 + \tilde{v}^2 = c^2. \tag{2.4}$$

3. The numerical method

Our numerical scheme uses a finite volume formulation with the original one-dimensional Roe approximate Riemann solver, extended to second order in space by use of a monotonized central-difference flux limiter, and a Lax–Wendroff-type correction to achieve second-order accuracy in time (LeVeque 1997). The Roe averages are used to compute the numerical fluxes, with no sonic fix. The one-dimensional solver is second-order accurate in space and time, while the overall scheme is formally first-order accurate in time due to dimensional splitting.

To remove errors caused by numerical dispersion at the shocks, we apply a monotonized central-difference flux limiter to the wave amplitudes in the approximate Riemann solution throughout the domain.

We solve the shock reflection problem numerically in a reference frame moving with the incident shock, and use a slanted grid whose coordinate lines are aligned with the shock and the wall. As well as minimizing the size of the computational domain, this grid gives a single-point transition for the incident shock, since a stationary grid-aligned shock is an exact solution of the Roe scheme. The exact representation of the incident shock on the grid eliminates small initial waves and oscillations produced by the flux limiter, thus preventing the contamination of the solution near the triple point by numerical oscillations. The computational cell is a parallelogram, and Riemann problems are solved in the directions normal to the cell edges.

In order to resolve the solution near the triple point, we use a block adaptive grid refinement technique described by Berger & Colella (1989). It would be computationally expensive to use refined grids around all three shocks throughout the domain, so we use grid refinement only around the triple point. As a result, the shocks cross grid interfaces where the numerical viscosity is discontinuous. We need to take special care to prevent the generation of diffusion waves and oscillations when this happens.

No waves are generated by the stationary incident shock, because it is an exact solution of the numerical equations at all grid levels. The reflected shock becomes very weak as it propagates away from the triple point, and the solution in the reflected wave is sensitive to the effect of numerical diffusion that propagates from coarse to fine levels. We make the distances between the boundaries of successively refined regions large enough to reduce this source of error to an acceptable level. The Mach shock becomes stronger as it moves away from the triple point and toward the wall. Since the Mach shock moves slowly with respect to the grid, the effect of numerical diffusion on it is small. We eliminate wave reflections when the Mach shock crosses the grid interfaces by using a flux limiter at the lower grid boundary that reduces the second-order space interpolation from coarse to fine grids to first order. Small oscillations are generated by the flux limiter in the region near the wall where the Mach shock is at a significant angle to the grid lines. This region is far from the triple point, and these oscillations do not propagate into the triple point region.

Initially, all the grids have their lower boundary located on the wall, and contain the point where the incident shock hits the wall, as illustrated in figure 2. The outflow boundary condition is used for $x < 0.15$. For $t > 0$, a triple point forms and moves up the incident shock. We move the refined grids independently to keep the triple point centred. It is crucial to keep the triple point inside the finest grid region. If we refined an initially coarse grid at later times, we would just obtain a highly resolved coarse solution.

We validated the code by carrying out convergence studies using various time and space mesh sizes. We also compared our results with the previous computations of

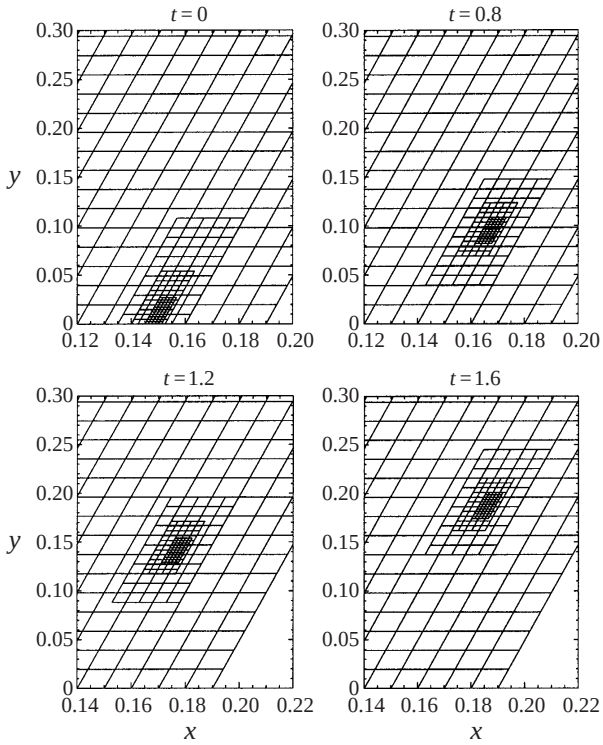

FIGURE 2. Time evolution of grid levels $l = 0$–3 in the adaptive grid structure.

	ρ	u	v	p
left	1.060	−1.295	−0.015	1.102
right	1.00	−1.37	0.00	1.00

TABLE 1. Initial conditions for the density ρ, x-velocity u, y-velocity v, and pressure p to the left and right of the incident shock. The initial location of the shock is $x = (\tan\theta_w)y$ with $\theta_w = 11.46°$.

Colella & Henderson (1990). To verify the self-similarity of the solution, we checked the constant velocity vector of the triple point and linear time dependence of the horizontal distance from the triple point to the sonic line.

The solution contains very weak shocks, a tiny supersonic patch, and a very weak expansion wave, so it is a good test problem for checking the accuracy and sensitivity of a numerical scheme.

4. Results

We consider initial data that correspond to a shock with Mach number $M = 1.04$, at an angle of incidence $\theta_w = 11.46°$ to the normal of a wall. Table 1 gives the initial values of the fluid variables in the reference frame described in the previous section.

Figure 3 shows a numerical solution of equations (2.1) that gives an overall picture of the Mach reflection. For clarity, only the boundaries of the first three of the six refined grids are shown. The coarse level ($l = 0$) consists of 400×400 points on a

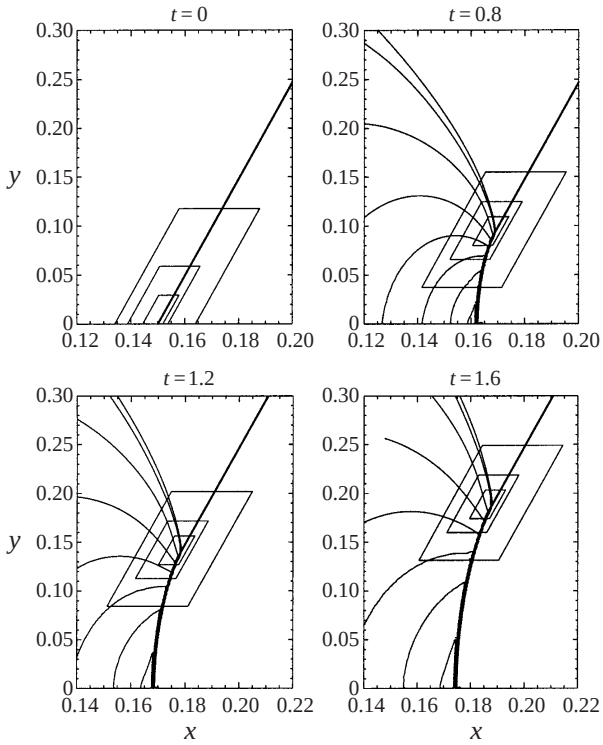

FIGURE 3. Density contours on grid levels $l = 0$–3.

parallelogram of size 0.2×0.4. The subsequent refined levels ($l = 1$ to 6) each have 120×240 points and a refinement ratio of 2 in each dimension, starting with a level $l = 1$ grid of size 0.03×0.12. The triple point location at time $t = 1.6$ is $y \approx 0.1882$. The reflected shock is much weaker than the incident shock, with a Mach number of approximately 1.003 at the triple point. The large-scale structure of the solution is very similar to that obtained by Colella & Henderson (1990) for weak shock reflection off a wedge. Their solution, however, uses only one level of grid refinement, and it is not sufficiently resolved to reveal the structure of the solution near the triple point.

Figure 4 shows the density contours on the three most refined grids, and figure 5 shows the density contours on the finest grid. The dashed line in figure 5 is the numerically computed location of the sonic line, equation (2.4). The sonic line bends back into the reflected wave and there is a very small supersonic patch behind the triple point. The supersonic patch is approximately 0.00015 wide in x and 0.001 high in y. This height is approximately 0.5% of the height of the Mach stem.

As in the numerical solution of the unsteady transonic small-disturbance equations in Hunter & Brio (2000), we find that the main effect of increasing numerical resolution is that the dip of the density contours and the sonic line toward the triple point becomes more pronounced. The widths of the shocks shrink with increasing resolution, but the width of the supersonic patch remains almost the same, even increasing slightly. This increase in size is presumably a result of the reduction of numerical diffusion due to grid refinement, and shows that the patch is not an artifact of numerical diffusion.

Henderson & Menikoff (1998) show that if three shocks meet at a point, then

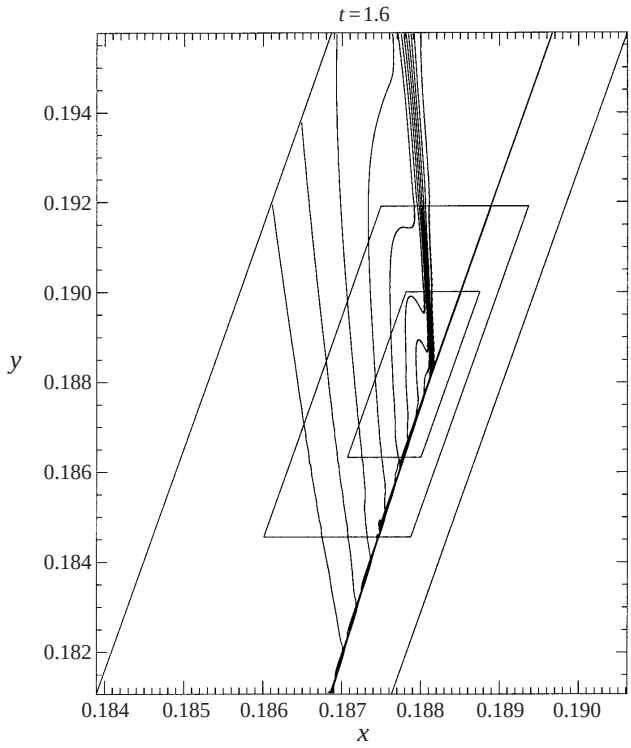

FIGURE 4. Density contours on grid levels $l = 4$–6.

they generate a contact discontinuity. Moreover, a configuration with three shocks and a contact discontinuity is impossible for weak shocks, of the strength found in this solution (Henderson 1987). Therefore we conjecture that the local structure consists of three shocks, a contact discontinuity, and an expansion fan meeting at the triple point. The jumps in the entropy and tangential velocity across the contact discontinuity are so small, however, that we cannot see them directly in the numerical solution. The density contours that dip toward the sonic point may be interpreted as the density contours of an expansion fan whose corner is smoothed out by numerical diffusion.

This structure is similar to the structure proposed previously in several different problems involving triple points (Li & Ben-Dor 1997; Bleakney & Taub 1949; Guderley 1962; Hunter & Brio 2000). The supersonic patch and the fan are embedded inside an apparently continuous self-similar diffracted wave pattern behind the triple point. Thus, the expansion fan is not a simple centred Prandtl–Meyer expansion fan that separates constant states.

In the hyperbolic region, the self-similar equations have two families of sound wave characteristics. Figures 6 and 7 show the numerically computed characteristic vector fields, of equation (2.3), for the solution inside the supersonic patch at the finest grid level. The minus characteristics cross the shocks, while plus characteristics converge on all three shocks.

In the weak-shock limit, the transition from regular to Mach reflection occurs when the shock strength $M-1$ and the angle θ_w of the shock to the wall normal are related by (2.2). In this limit, the Euler equations may be approximated by the unsteady

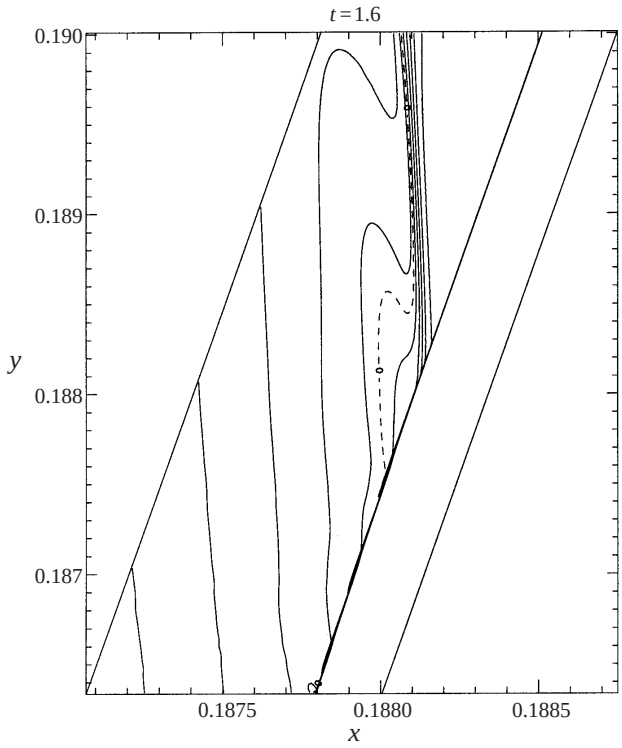

FIGURE 5. Density contours and sonic line (dashed) on grid level $l = 6$. The parallelogram shown is covered by a 120×240 grid.

transonic small-disturbance equations. Because of transonic similarity, the local flow pattern near the reflection and triple points depends on a single parameter,

$$a = \frac{\theta_w}{2\sqrt{M-1}}.$$

The parameter values $M = 1.04$ and $\theta_w = 11.46^\circ$, used above, correspond to $a = 0.5$.

A numerical solution of the asymptotic shock reflection problem for the unsteady transonic small-disturbance equation with $a = 0.5$ is shown in Hunter & Brio (2000). The unsteady transonic small-disturbance solution is remarkably similar to the Euler solution. For instance, compare figure 8 and figures 10–11 in Hunter & Brio (2000) with figure 5 and figures 6–7 here. Table 2 compares the values predicted from the unsteady transonic small-disturbance solution for several important quantities with the values obtained from the direct numerical solution. The values obtained using the unsteady transonic small-disturbance and Euler equations are in good agreement, although the size of the supersonic patch in the Euler solution is even smaller than predicted from the unsteady transonic small-disturbance solution. Exact agreement is not to be expected, since the unsteady transonic small-disturbance solution is only accurate to the order $M - 1$.

5. Conclusions

In this paper we have presented a numerical solution of the Euler equations for the Mach reflection of a weak shock in a half-space that uses adaptive grid refinement

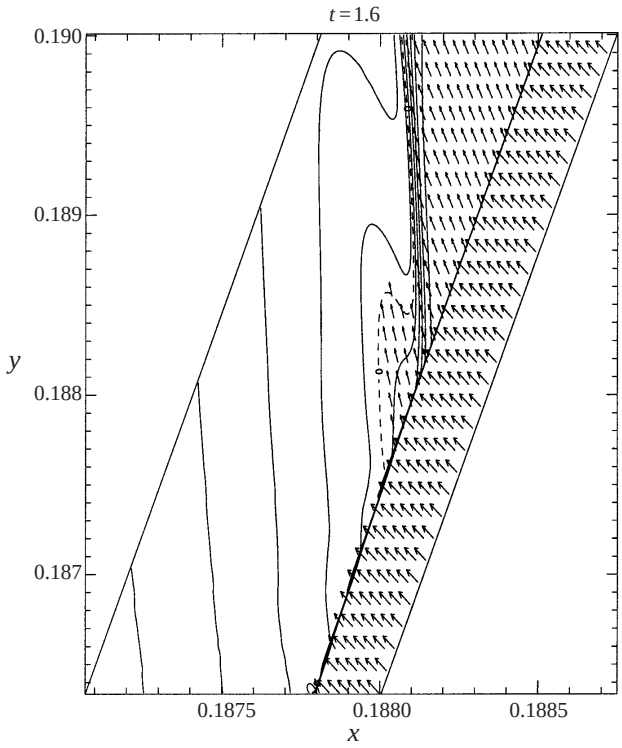

FIGURE 6. The minus characteristic vector field on grid level $l = 6$.

	Euler	UTSD
χ	4.8°	5.7°
M_{wall}	1.073	1.072
M_{ref}	1.003	1.0028
h_x	0.08%	0.1%
h_y	0.53%	1.0%

TABLE 2. Comparison of the numerical solutions of the Euler and unsteady transonic small disturbance (UTSD) equations for $M = 1.04$, $\theta_w = 11.46°$, and $\gamma = 5/3$. Here, χ is the angle of the triple point to the wedge, M_{wall} is the strength of the Mach shock at the wall, M_{ref} is the strength of the reflected shock at the triple point, h_x is the width of the supersonic patch along the wall, and h_y is the height of the patch normal to the wall, as a percentage of the Mach stem height.

near the triple point. The solution contains a tiny supersonic patch behind the triple point, as proposed by Guderley (1962). Our numerical solution of the Euler equations is in excellent agreement with the numerical solution in Hunter & Brio (2000) of the unsteady transonic small-disturbance equations.

For a shock with Mach number 1.04 at an angle of incidence of 11.46° in an ideal gas with $\gamma = 5/3$, the height of the supersonic patch is approximately 0.5% of the height of the Mach stem, and its width is five times smaller. The patch is embedded inside a diffracted wave pattern which is about five times larger than the patch itself.

The von Neumann triple point 'paradox' only arises with respect to an inviscid description of the fluid flow. As we have shown, the apparent paradox is resolved by

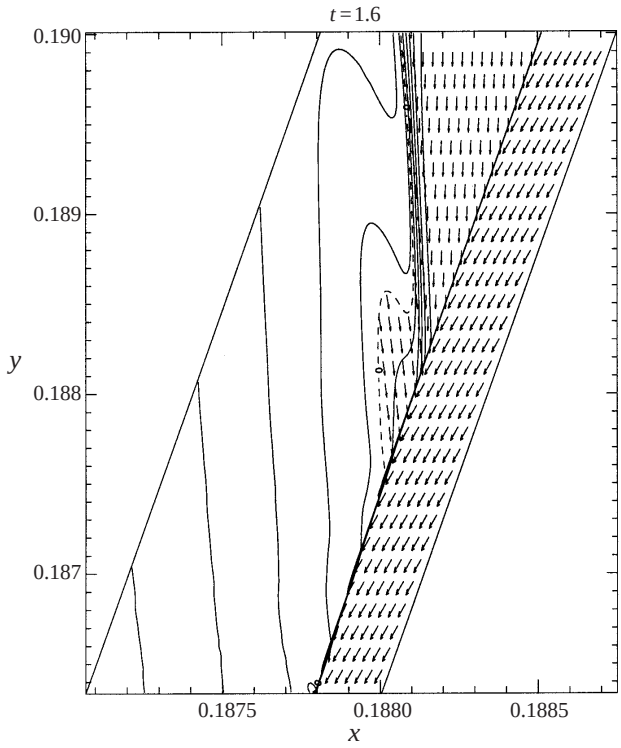

FIGURE 7. The plus characteristic vector field on grid level $l = 6$.

the existence of a tiny supersonic patch behind the triple point, and viscosity is not required to explain it, as has sometimes been suggested (Sternberg 1959).

In view of the extremely small size of the patch, it is natural to ask what the effect of viscosity is on the inviscid flow. Since the triple point lies in the interior of the fluid, it is reasonable to expect that boundary layer effects do not influence the local structure of the solution. Thus, the main effect of viscosity it to give the shocks a finite thickness. The thickness Δ of a weak shock of Mach number M is given approximately by (Thompson 1971)

$$\Delta = \frac{3}{M-1}\lambda,$$

where λ is the mean free path in the gas. For example, the mean free path in argon at standard conditions is given approximately by $\lambda = 6 \times 10^{-5}$ mm. Therefore for the values obtained in our computation, the reflected shock with Mach number $M = 1.003$, has a thickness of $\Delta = 6 \times 10^{-2}$ mm. The width W of the supersonic patch along the wall is given by $W = 8 \times 10^{-4}H$, where H is the height of the Mach stem. For a Mach stem height of $H = 100$ mm, we get $W = 8 \times 10^{-4}$ mm, and the supersonic patch has the same size as the reflected shock structure. For a Mach stem height of $W = 1$ m, the patch is an order of magnitude larger than the reflected shock thickness, and we expect that the viscous solution will approach the inviscid solution for large times. Moreover, we also expect a greater separation between the reflected shock strength and the patch width for stronger incident shocks, for example $M_s = 1.09$ and $\theta_w = 17.2^\circ$, which still corresponds to $a = 0.5$.

Now that the parameters and the size of the physical region in question are better known, we hope that an experimental observation of the patch will be possible.

The work of J. K. H. was partially supported by NSF under grant number DMS-9404155. G. M. W. was supported in part by NASA grant NAG5-5164.

Appendix

In this Appendix we derive equation (2.3) for the self-similar sound wave characteristics of the Euler equations, and equation (2.4) for the sonic line. See Courant & Hilbert (1989) and Webb *et al.* (1998) for a general discussion of characteristics, and Samtaney (1997) and Zhang & Zheng (1990) for a discussion of the self-similar Euler equations.

Self-similar solutions of the Euler equations (2.1) have the form

$$u = c_0 U(\xi,\eta), \quad v = c_0 V(\xi,\eta), \quad \rho = \rho_0 R(\xi,\eta), \quad p = p_0 P(\xi,\eta), \tag{A 1}$$

where $\boldsymbol{u} = (u, v)$ is the fluid velocity, and

$$\xi = \frac{x}{c_0 t}, \qquad \eta = \frac{y}{c_0 t} \tag{A 2}$$

are the similarity variables. The constants p_0 and ρ_0 are characteristic values of the pressure and density, and

$$c_0 = \left(\frac{\gamma p_0}{\rho_0}\right)^{1/2}$$

is the corresponding sound speed.

Use of (A 1) and (A 2) in (2.1) gives the system

$$\boldsymbol{A}^{(1)}\Psi_\xi + \boldsymbol{A}^{(2)}\Psi_\eta = 0,$$

where $\Psi = (R, U, V, P)^T$, and the matrices $\boldsymbol{A}^{(1)}$ and $\boldsymbol{A}^{(2)}$ are given by

$$\boldsymbol{A}^{(1)} = \begin{pmatrix} U-\xi & R & 0 & 0 \\ 0 & U-\xi & 0 & 1/(\gamma R) \\ 0 & 0 & U-\xi & 0 \\ 0 & \gamma P & 0 & U-\xi \end{pmatrix},$$

$$\boldsymbol{A}^{(2)} = \begin{pmatrix} V-\eta & 0 & R & 0 \\ 0 & V-\eta & 0 & 0 \\ 0 & 0 & V-\eta & 1/(\gamma R) \\ 0 & 0 & \gamma P & V-\eta \end{pmatrix}.$$

The curve $\varphi(\xi,\eta) = \text{const}$ is a characteristic of this system if

$$\det\left(\varphi_\xi \boldsymbol{A}^{(1)} + \varphi_\eta \boldsymbol{A}^{(2)}\right) = 0. \tag{A 3}$$

Computing the determinant of this matrix, we find that φ satisfies

$$\left[(U-\xi)\varphi_\xi + (U-\eta)\varphi_\eta\right]^2 \left\{\left[(U-\xi)\varphi_\xi + (U-\eta)\varphi_\eta\right]^2 - \hat{c}^2\left(\varphi_\xi^2 + \varphi_\eta^2\right)\right\} = 0,$$

where

$$\hat{c} = \left(\frac{P}{R}\right)^{1/2}$$

is a non-dimensionalized sound speed. Solutions of the equation

$$\left[(U-\xi)\varphi_\xi + (U-\eta)\varphi_\eta\right]^2 = 0$$

are associated with entropy and vorticity waves, and solutions of

$$\left[(U-\xi)\varphi_\xi + (U-\eta)\varphi_\eta\right]^2 - \hat{c}^2(\varphi_\xi^2 + \varphi_\eta^2) = 0 \tag{A 4}$$

are associated with sound waves. Writing

$$\boldsymbol{z} = \begin{pmatrix}\xi\\ \eta\end{pmatrix}, \qquad \tilde{\boldsymbol{U}} = \begin{pmatrix}U-\xi\\ V-\eta\end{pmatrix},$$

we find that the characteristics of (A 4) are given by

$$\frac{\mathrm{d}\boldsymbol{z}}{\mathrm{d}\tau} = \tilde{\boldsymbol{U}} \pm \hat{c}\boldsymbol{n}, \qquad \frac{\mathrm{d}\varphi}{\mathrm{d}\tau} = 0, \tag{A 5}$$

where τ is a parameter along the characteristics, and

$$\boldsymbol{n} = (\varphi_\xi^2 + \varphi_\eta^2)^{-1/2}\begin{pmatrix}\varphi_\xi\\ \varphi_\eta\end{pmatrix}$$

is the unit normal to the curve $\varphi = \text{const}$. On the self-similar sound wave characteristics, (A 5), we have

$$\boldsymbol{n}\cdot\mathrm{d}\boldsymbol{z} = 0, \qquad (\tilde{\boldsymbol{U}} \pm \hat{c}\boldsymbol{n}) \times \mathrm{d}\boldsymbol{z} = 0. \tag{A 6}$$

Writing

$$\tilde{\boldsymbol{U}} = |\tilde{\boldsymbol{U}}|\begin{pmatrix}\cos\alpha\\ \sin\alpha\end{pmatrix}, \quad \mathrm{d}\boldsymbol{z} = |\mathrm{d}\boldsymbol{z}|\begin{pmatrix}\cos\theta\\ \sin\theta\end{pmatrix}, \quad \boldsymbol{n} = \begin{pmatrix}-\sin\theta\\ \cos\theta\end{pmatrix},$$

we obtain from the second equation in (A 6) the Mach cone equation

$$\sin(\theta-\alpha) = \frac{\pm\hat{c}}{\left[(U-\xi)^2 + (V-\eta)^2\right]^{1/2}}. \tag{A 7}$$

If $(U-\xi)^2 + (V-\eta)^2 \geqslant \hat{c}^2$, then the flow is supersonic, and the solution of (A 7) is

$$\theta = \alpha \pm \arcsin\left(\frac{\hat{c}}{[(U-\xi)^2 + (V-\eta)^2]^{1/2}}\right).$$

Rewriting this equation as a differential equation for $\mathrm{d}\eta/\mathrm{d}\xi$, we get equation (2.3) in § 2. The sonic line,

$$(U-\xi)^2 + (V-\eta)^2 = \hat{c}^2,$$

separates the supersonic region, with real sound wave characteristics, from the subsonic region, with complex sound wave characteristics.

REFERENCES

Berger, A. & Colella, P. 1989 Local adaptive mesh refinement for shock hydrodynamics. *J. Comput. Phys.* **82**, 64–84.

Bleakney, W. & Taub, A. H. 1949 Interaction of shock waves. *Rev. Modern Phys.* **21**, 584–605.

Colella, P. & Henderson, L. F. 1990 The von Neumann paradox for the diffraction of weak shock waves. *J. Fluid Mech.* **213**, 71–94.

Courant, R. & Hilbert, D. 1989 *Methods of Mathematical Physics*. Wiley.

Guderley, K. G. 1962 *The Theory of Transonic Flow*. Pergamon.

Henderson, L. F. 1987 Regions and boundaries for diffracting shock wave systems. *Z. Angew. Math. Mech.* **67**, 73–86.

Henderson, L. F. & Menikoff, R. 1998 Triple-shock entropy theorem and its consequences. *J. Fluid Mech.* **366**, 179–210.

Hunter, J. K. & Brio, M. 2000 Weak shock reflection. *J. Fluid Mech.* **410**, 235–261.

LeVeque, R. J. 1997 Wave propagation algorithms for multidimensional hyperbolic systems. *J. Comput. Phys.* **131**, 327–353.

Li, H. & Ben-Dor, G. 1997 Analytical investigation of two-dimensional unsteady shock-on-shock interaction. *J. Fluid Mech.* **340**, 101–128.

Neumann, J. von 1963 *Collected Works*, vol. 6. Pergamon.

Samtaney, R. 1997 Computational methods for self-similar solutions of the compressible Euler equations. *J. Comput. Phys.* **132**, 327–345.

Sternberg, J. 1959 Triple-shock-wave intersections. *Phys. Fluids* **2**, 179–206.

Tesdall, A. M. & Hunter, J. K. 2000 Self-similar solutions for weak shock reflection. In preparation.

Thompson, P. A. 1971 *Compressible Fluid Dynamics.* McGraw-Hill.

Webb, G. M., Ratkiewicz, R., Brio, M. & Zank, G. P. 1998 Multidimensional simple waves in gas dynamics. *J. Plasma Phys.* **59**, 417–460.

Zhang, T. & Zheng, Y. 1990 Conjecture on the structure of solutions of the Riemann problem for two-dimensional gas dynamics systems. *SIAM J. Math. Anal.* **21**, 593–630.